the use of the TFQMR method, the algorithm avoids the computation of the multiplication between the transpose of the system matrix and a vector, which is required in both the CG–FFT and BCG–FFT methods. As a result, the programming complexity is greatly reduced. Furthermore, since on average the TFQMR method requires only one matrix-by-vector multiplication, which can be evaluated using six FFT's, the TFQMR–FFT algorithm is more efficient than the currently available CG–FFT and BCG–FFT methods.

## REFERENCES


[1] D. E. Livesay and K. M. Chen, "Electromagnetic fields induced inside arbitrarily shaped biological bodies," *IEEE Trans. Microwave Theory Tech.*, vol. MTT-22, pp. 1273–1280, Dec. 1974.

[2] D. H. Schaubert, D. R. Wilton, and A. W. Glisson, "A tetrahedral modeling method for electromagnetic scattering by arbitrarily shaped inhomogeneous dielectric bodies," *IEEE Trans. Antennas Propagat.*, vol. AP-32, pp. 77–85, Jan. 1984.

[3] R. D. Graglia, P. L. E. Uslenghi and R. S. Zich, "Moment method with isoparametric elements for three-dimentional anisotropic scatters," *Proc. IEEE*, vol. 5, pp. 750–760, July 1989.

[4] N. N. Bojarski, "$\bar{K}$-Space formulation of the electromagnetic scattering problems," Air Force Avionic Lab. Tech. Rep. AFAL-TR-71-75, 1971.

[5] D. T. Borup and O. P. Gandhi, "Fast-Fourier transform method for calculation of SAR distributions in finely discretized inhomogeneuos models of biological bodies," *IEEE Trans. Microwave Theory Tech.*, vol. MTT-32, pp. 355–360, Apr. 1984.

[6] T. K. Sarkar, E. Arvas, and S. M. Rao, "Application of FFT and the conjugate gradient method for the solution of electromagnetic radiation from electrically large and small conducting bodies," *IEEE Trans. Antennas Propagat.*, vol. AP-34, pp. 635–640, May 1986.

[7] J. M. Jin and J. L. Volakis, "A biconjugate gradient FFT solution for scattering by planar plates," *Electromagnetics*, vol. 12, no. 1, pp. 105–119, 1992.

[8] M. F. Catedra, E. Gago, and L. Nuno, "A numerical scheme to obtain the RCS of three-dimensional bodies of size using the conjugate gradient method and the fast Fourier transform," *IEEE Trans. Antennas Propagat.*, vol. 37, pp. 528–537, Apr. 1989.

[9] C. Y. Shen, K. J. Glover, M. I. Sancer, and A. D. Varvatsis, "The discrete Fourier transform method of solving differential-integral equations in scattering theory," *IEEE Trans. Antennas Propagat.*, vol. 37, pp. 1032–1041, June 1989.

[10] P. Zwamborn and P. M. van der Berg, "The three-dimensional weak form of the conjugate gradient FFT method for solving scattering problems," *IEEE Trans. Microwave Theory Tech.*, vol. 40, pp. 1757–1766, Sept. 1992.

[11] A. P. M. Zwamborn, P. M. van der Berg, J. Mooibroek, and F. T. C. Koenis, "Computation of three-dimensional electromagnetic-fields distributions in a human body using the weak form of the CGFFT method," *ACES J.*, vol. 7, pp. 26–42, 1992.

[12] A. P. M. Zwamborn and P. M. van der Berg, "Computation of electromagnetic fields inside strongly inhomogeneous objects by the weak-conjugate-gradient fast-Fourier-transform method," *J. Opt. Soc. Amer. A, Opt. Image Sci.*, vol. 11, pp. 1414–1420, 1994.

[13] H. Gan and W. C. Chew, "A discrete BCG-FFT algorithm for solving 3D inhomogeneous scattering problems," *J. Electromagn. Wave Applicat.*, vol. 9 , no. 10, pp. 1339–1357, 1995.

[14] J. H. Lin and W. C. Chew, "BiCG-FFT T-matrix method for the scattering solution from inhomogeneous bodies," *IEEE Trans. Microwave Theory Tech.*, vol. 44, pp. 1150–1155, July 1996.

[15] R. W. Freund, "A transpose-free quasiminimal residual algorithm for non-Hermitian linear systems," *SIAM J. Sci. Stat. Comput.*, vol. 14, no. 2, pp. 470–482, 1993.

[16] R. W. Freund and N. M. Nachtigal, "A quasiminimal residual method for non-Hermitain linear systems," *Numer. Math.*, vol. 60, pp. 315–339, 1991.

[17] P. Sonneveld, "CGS, a fast Lanczos-type solver for nonsymmetric linear systems," *SIAM J. Sci. Stat.. Comput.*, vol. 10, pp. 36–52, 1989.

[18] H. A. van Der Vorst, "BI-CGSTAB: A fast and smoothly converging variant of BI-CG for the solution of nonsymmetric linear systems," *SIAM J. Sci. Stat. Comput.*, vol. 13, pp. 631–644, 1992.

[19] T. F. Chan, E. Gallopoulos, V. Simoncini, T. Szeto, and C. H. Tong, "A quasiminimal residual variant of the BI-CGSTAB algorithm for nonsymmetric systems," *SIAM J. Sci. Stat. Comput.*, vol. 15, no. 2, pp. 338–347, 1994.

[20] Y. Saad, *Iterative Method for Sparse Linear Systems*. New York: PWS, 1995.

[21] P. J. Dimbylow and S. M. Mann, "SAR calculations in an anatomically realistic model of the head for mobile communication transceivers at 900 MHz and 1.8 GHZ," *Phys. Med. Biol.*, vol. 39, pp. 361–368, 1994.

[22] J. M. Jin, J. Chen, H. Gan, W. C. Chew, R. L. Magin, and P. J. Dimbylow, "Computation of electromagnetic fields for high-frequency magnetic resonance imaging applications," *Phys. Med. Biol.*, vol. 41, pp. 2719–2738, 1996.


# Two-Dimensional Wavelet-Analysis of a Microstrip Open

Gerald Oberschmidt, Karsten Bubke, and Arne F. Jacob

***Abstract*— Simple two-dimensional (2-D) wavelet systems are used in a moment method to analyze a microstrip discontinuity. This allows one to efficiently compress the impedance matrix. The achievable sparsity is discussed for different resolution depths where up to 85% was obtained for an error below 1%.**

***Index Terms*— Matrix compression, numerical analysis, planar microwave circuits, wavelets.**

## I. INTRODUCTION

The spectral-domain moment method is known to be a very effective tool for the analysis of planar microwave circuits [1]. It leads, however, to densely populated impedance matrices. For large or complex circuit configurations, this can become a serious problem because of limited computer resources. This drawback can be overcome by discretizing with wavelet bases because they allow compression of the impedance matrices [2]–[5].

Wavelet bases have recently been used to effectively analyze two-dimensional (2-D) structures [3]. Here, the wavelet scheme has been extended to two dimensions, similar to [6].

After briefly reviewing the method and the concept of wavelets, we present the construction of tensor wavelets in two dimensions with arbitrary resolution levels in both directions. Details about the implementation of the program are followed by a discussion of the results.

## II. METHOD

To analyze an open microstrip line, the electric-field integral equation (EFIE) is solved in the spectral domain [1]. Since for electrically narrow strips the transverse current can be neglected [3], the EFIE reduces to

$$\tilde{E}_x(\alpha, \beta, h) = \tilde{G}_{xx}(\alpha, \beta)\tilde{J}_x(\alpha, \beta, h) \tag{1}$$

for the longitudinal components of the electric field and current density. Here, $\alpha$ and $\beta$ are the $x$- and $y$-space frequencies, respectively, and $h$ is the height of the substrate. The tilde denotes the Fourier transform. Definitions and notations, especially for the Green's function $\tilde{G}_{xx}$, are as in [1].

Manuscript received September 30, 1996; revised February 14, 1998.

The authors are with the Institut für Hochfrequenztechnik, Technische Universität Braunschweig, 38023 Braunschweig, Germany (e-mail: G.Oberschmidt@tu-bs.de; A.Jacob@tu-bs.de).

Publisher Item Identifier S 0018-9480(98)03170-6.

Applying a Galerkin Method to the integral equation yields the system of linear equations

$$\overline{\overline{g}}_{xx}\vec{j}_x = \vec{e}_x \tag{2}$$

with the moment matrix $\overline{\overline{g}}_{xx}$ and the coefficient vectors $\vec{j}_x$ and $\vec{e}_x$. Accuracy and efficiency of the analysis strongly depend on the choice of the basis functions. For physical reasons, they must ensure current continuity in the longitudinal direction, but may allow a discontinuous distribution along the transverse axis. For complicated geometries, sub-domain functions are well suited. Wavelet bases have proven to be very effective [2].

## III. Wavelet Analysis

To introduce wavelets, let us briefly review the concept of the multiresolutional analysis (MRA), which is fundamental for the application of wavelets [7]–[9].

The projection $P_m f$ of a function $f$ on a resolution level $m$ is determined by the coefficients $c_l$ through

$$P_m f(t) = \sum_{l=-\infty}^{\infty} c_l \phi(2^m t - l). \tag{3}$$

Here, $\phi(2^m t - l)$ are the scaling functions which span the coarse space $\mathbf{V}_m \subset \mathbf{L}^2$—the space of square integrable functions. For a finer approximation $P_{m+1} f$ on $\mathbf{V}_{m+1}$, a detail space $\mathbf{W}_m$ (the orthogonal complement of $\mathbf{V}_m$ in $\mathbf{V}_{m+1}$) is introduced. The basis functions of $\mathbf{W}_m$ are the wavelets $\sqrt{2^m}\psi(2^m t - l)$. The wavelets have at least one vanishing moment. Wavelets and scaling functions can be constructed from finer scaling functions via the refinement relations

$$\{\phi(t),\ \psi(t)\}^T = \sum_{l=-\infty}^{\infty} \{h_l^{\phi},\ h_l^{\psi}\}^T \phi(2t - l). \tag{4}$$

Here, the filter coefficients $h_i^{\phi}$, $h_i^{\psi}$ do not only uniquely define the wavelet bases, but also the decomposition of a function into them [7]. The projection $P_M f$ can thus be decomposed as

$$P_M f = \sum_{n=-\infty}^{\infty} c_n \phi(2^{m_0} t - n) + \sum_{m=m_0}^{M-1} \sum_{n=-\infty}^{\infty} d_{mn} \psi(2^m t - n) \tag{5}$$

with the starting resolution $m_0$. Coefficients $\{d_{mn}\}$ denote the amplitudes of the wavelets. Whereas the scaling functions cover the low-frequency content, the wavelets include the information in their respective frequency band.

Various families of wavelet bases have been developed and used [7]–[9]. Among the simplest, the Haar-basis and the Chui–Wang wavelets [9] were shown to suffice for the analysis of planar structures [5]. Additionally, since both can be adapted to bounded intervals [4], [5], they were used in this paper.

In the Haar system, scaling functions and wavelets are given by

$$\phi_1(t) = \begin{cases} 1, & 0 < t < 1 \\ 0, & \text{otherwise} \end{cases}$$

$$\psi_1(t) = \begin{cases} 1, & 0 < t < \frac{1}{2} \\ -1, & \frac{1}{2} < t < 1 \\ 0, & \text{otherwise.} \end{cases} \tag{7}$$

Their filter coefficients are $h_0^{\phi} = h_1^{\phi} = 1$ and $h_0^{\psi} = -h_1^{\psi} = 1$. It can easily be verified that the Haar system forms an orthogonal basis. Restriction to a bounded interval is achieved by simply omitting the functions outside the region of interest. The Chui–Wang system of piecewise linear functions is generated by the hat function defined on the interval $[0, \cdots, 2]$ as follows:

$$\phi_2(t) = \begin{cases} t, & 0 < t \le 1 \\ 2 - t, & 1 < t \le 2 \\ 0, & \text{otherwise.} \end{cases} \tag{8}$$

The filter coefficients are $\{h_0^{\phi},\ h_1^{\phi},\ h_2^{\phi}\} = \{1/2,\ 1,\ 1/2\}$ and $\{h_0^{\psi},\ h_1^{\psi},\ h_2^{\psi},\ h_3^{\psi},\ h_4^{\psi}\} = \{1/12,\ -1/2,\ 5/6,\ -1/2,\ 1/12\}$. In order to obtain a complete basis with homogeneous boundary conditions on a bounded interval, the functions extending over the limits need to again be omitted.

In [4], boundary wavelets with a jump discontinuity at the edges are employed. Here, however, we need wavelets to model the homogeneous current at the ends of the strip. Moreover, the boundary wavelets should have minimum support in the space $\mathbf{W}_m$. In the system of piecewise linear functions, three fine scaling functions suffice. Filter coefficients (4) are found by explicitly enforcing orthogonality to $\phi(2^m t - l) \in \mathbf{V}_m$ and normalizing the new wavelet. The coefficients for the left boundary wavelet are $\{h_0^{\psi_L},\ h_1^{\psi_L},\ h_2^{\psi_L}\} = \{1,\ -2/3,\ 1/9\}$.

A 2-D basis is needed to simulate the current distribution on the microstrip. In contrast to [3] where the transverse dependence of the longitudinal current distribution was modeled by a cubic term, we use a truly 2-D wavelet system. This can be derived from one-dimensional wavelets in the $x$- and $y$-direction by means of the tensor product [7]

$$\begin{pmatrix} [\phi^x_{m_0^x}(x-l)]_{l=1,\,N^{x,\phi}_{m_0^x}} \\ \{[\psi^x_m(x-l)]_{l=1,\,N^{x,\psi}_m}\}_{m=m_0^x,\,M^x} \end{pmatrix} \times \begin{pmatrix} [\phi^y_{m_0^y}(y-l)]_{l=1,\,N^{y,\phi}_{m_0^y}} \\ \{[\psi^y_m(y-l)]_{l=1,\,N^{y,\psi}_m}\}_{m=m_0^y,\,M^y} \end{pmatrix}^T. \tag{9}$$

Here, $m_0^{x,\,y}$ and $M^{x,\,y}$ define the coarsest and finest resolution levels, respectively. $N_m^{(x,\,y),(\phi,\,\psi)}$ denote the number of functions on resolution level $m$. The superscripts are self-explanatory. The resolution depth can be set independently in both directions for optimum decomposition of each current distribution. The wavelet system for the transverse distribution is the Haar system, whereas an approximation with a continuous system is needed in the longitudinal direction (Chui–Wang).

In this paper, we calculated the reaction integrals on the finest scaling function level and then decomposed the impedance matrix into different wavelet levels. This procedure is advantageous because as it exploits the translation symmetries of the rooftop functions, only $N_x \times N_y$ simple reaction integrals have to be computed. The transformation into a wavelet-Galerkin matrix is performed following the scheme

$$\overline{\overline{g}}^{WL}_{xx} = \overline{\overline{W}}\,\overline{\overline{g}}_{xx}\,\overline{\overline{W}}^T \tag{10}$$

where $\overline{\overline{W}}$ is set up from the filter coefficients in (4) and (9). The matrix multiplication can be accelerated because of the sparsity of $\overline{\overline{W}}$ and by employing a pyramid algorithm [7].

## IV. Results

The reaction integrals are calculated following the procedure outlined in [10]. The excitation of the fundamental mode is realized as in [11]. Finally, the propagation constant and the fundamental mode reflection coefficient $R$ are deembedded by means of a modal analysis with a matrix pencil method that was adapted from [12].

In a first example, the reflection coefficient of an open microstrip line (TRL 1) with substrate thickness $h = 0.635$ mm, strip width $b = 0.6$ mm, and dielectric constant $\epsilon_r = 9.9$ was calculated. The length of the line is $l = 10$ mm. The results were found to be in good agreement with those given in [3], as illustrated in Fig. 1. The slight discrepancy between the methods at high frequencies is due to the choice of the discretization of the current distribution. In particular, in [3], a cubic term was chosen for the transverse dependence.

The effect of thresholding on the impedance matrix sparsity (percentage of zero elements) is shown in Fig. 2 for four different cases. Here, the threshold defines (relative to the magnitude of the

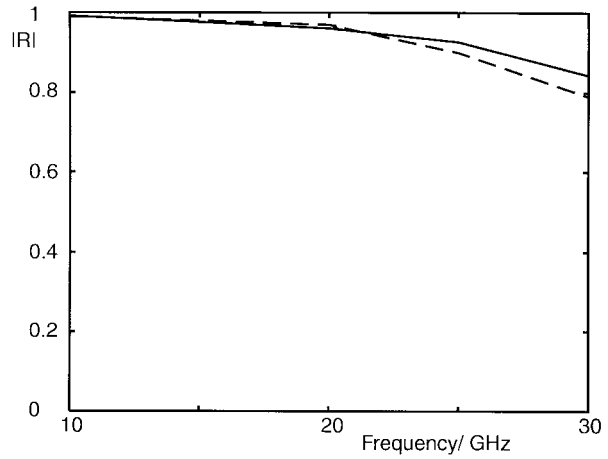


Fig. 1. Reflection coefficient of the microstrip open TRL 1 versus frequency. This paper: (—), after [3]: (- - -).

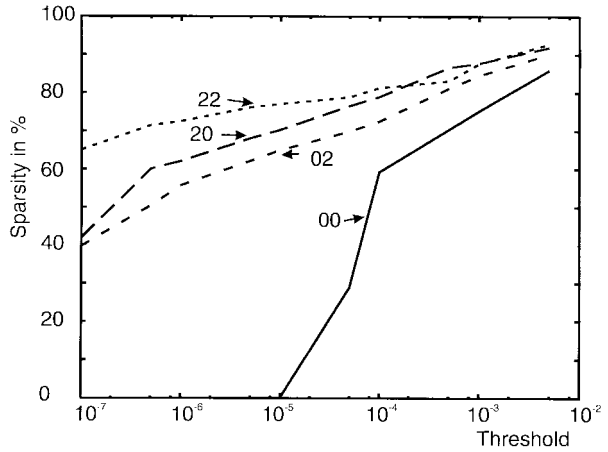


Fig. 2. Matrix sparsity versus threshold for different MRA levels denoted by $i$, $j$, the wavelet levels in longitudinal and transverse direction.

largest matrix element) the value below which elements are set to zero. The number of basis functions was 63 in the longitudinal direction and four in the transverse direction. For a classical basis (00), no elements vanish for a threshold below $10^{-5}$. The two digits denote the number of wavelet levels in the longitudinal and transverse direction, respectively. Observe the steep ascent of the sparsity around this value. After a wavelet transformation has been performed, the magnitude of the elements varies in a much wider range. More than 40% of the matrix elements are below a threshold of $10^{-7}$. It has been observed here that thresholding is most effective when the wavelet transformation is applied with two wavelet levels in both directions (22). But even in just one direction, (20) or (02), matrix compression can be done efficiently.

To illustrate the effects of compression on the reflection coefficient, Fig. 3 shows the relative deviation of its magnitude from $|R_0|$, the value without thresholding. The maximum allowable error was set to 1%. Again, a wavelet transformation in both directions (22) is superior to a compression in only one direction (02), (20), and the sparsity reaches 80%. For a single wavelet level, the figure remains slightly lower. Without wavelet transformation, an error of 1% is reached at a sparsity of approximately 45%. The phase deviation (not shown here) remains below $2^\circ$ up to a sparsity of more than 85% in the case of (22).

The sparsities and thresholds for an error of 1% in the magnitude of the reflection coefficient are listed in Table I. Here, not only

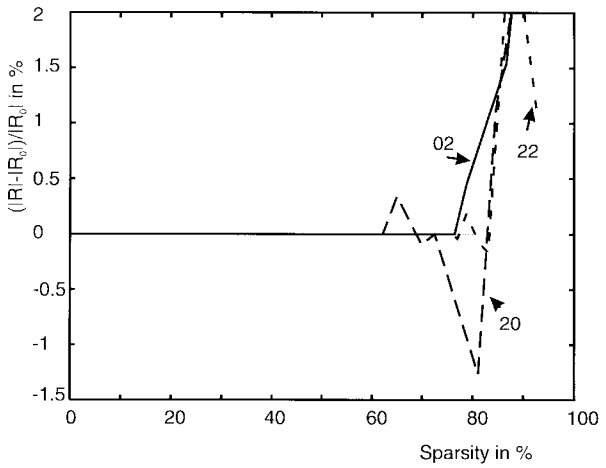


Fig. 3. Magnitude of the reflection coefficient versus sparsity for different MRA levels.

TABLE I
SPARSITY AND THRESHOLD FOR VARIOUS MRA LEVELS AND TWO DIFFERENT LINES FOR 1% ERROR IN $|R|$. NOTATIONS ARE AS IN FIG. 2

| | TRL 1 | | TRL 2 | |
|---|---|---|---|---|
| MRA | Sp.(%) | Threshold | Sp.(%) | Threshold |
| 00 | 45 | $4.5 \cdot 10^{-5}$ | 23 | $1.5 \cdot 10^{-5}$ |
| 01 | 79 | $1.4 \cdot 10^{-4}$ | 67 | $2.4 \cdot 10^{-5}$ |
| 02 | 78 | $1.1 \cdot 10^{-4}$ | 76 | $2.4 \cdot 10^{-5}$ |
| 03 | | | 81 | $5.3 \cdot 10^{-5}$ |
| 10 | 67 | $8.8 \cdot 10^{-5}$ | 63 | $2.7 \cdot 10^{-5}$ |
| 20 | 79 | $2.3 \cdot 10^{-4}$ | 55 | $1.1 \cdot 10^{-5}$ |
| 30 | | | 48 | $6.1 \cdot 10^{-6}$ |
| 11 | 85 | $3.4 \cdot 10^{-4}$ | 71 | $1.9 \cdot 10^{-5}$ |
| 22 | 84 | $9.5 \cdot 10^{-4}$ | 70 | $1.2 \cdot 10^{-4}$ |

different MRA depths are compared, but also another microstrip line (TRL 2: $h = 0.15\,\text{mm}$, $b = 1.5\,\text{mm}$, $\epsilon_r = 12.8$, $l = 10\,\text{mm}$, $f = 20\,\text{GHz}$) with a width-to-height ratio of 10 has been included for further comparison. Also, the number of functions has been varied: instead of $63 \times 4$, we employed $31 \times 8$ functions. This corresponds to a longitudinal discretization of about 13 functions per effective wavelength—already a rather coarse approximation. Thus, there is not much redundancy in the longitudinal direction, resulting in a poorer compression of the matrix (see Table I, MRA 10, 20, 30). In the transverse direction, the finer grid leads to more redundancy and thus allows for a more efficient matrix compression (see Table I, MRA 01, 02, 03). Adding wavelet levels in longitudinal direction does not significantly alter the obtained sparsity (see Table I, MRA 11, 22).

## V. CONCLUSION

A wavelet scheme using simple wavelets has been extended to two dimensions. This basis is employed in a spectral-domain moment method to analyze a microstrip discontinuity. It has been shown that wavelets are an effective tool for compressing the impedance matrix, particularly when starting with a fine discretization because, for instance, when an appropriate resolution is not known *a priori*, wavelets will adaptively find and reduce redundancy.

## REFERENCES

[1] T. Uwano and T. Itoh, "Spectral domain approach," in *Numerical Techniques for Microwave and Millimeter-Wave Passive Structures*, T. Itoh, Ed. New York: Wiley, 1989, pp. 335–380.

[2] K. Sabetfakhri and L. P. B. Katehi, "Analysis of integrated millimeter-wave and submillimeter-wave waveguides using orthonormal wavelet

expansions," *IEEE Trans. Microwave Theory Tech.*, vol. 42, pp. 2412–2422, Dec. 1994.
[3] G. Wang and G. W. Pan, "Full wave analysis of microstrip floating line structures by wavelets expansion method," *IEEE Trans. Microwave Theory Tech.*, vol. 43, pp. 131–142, Jan. 1995.
[4] J. C. Goswami, A. K. Chan, and C. K. Chui, "On solving first-kind integral equations using wavelets on a bounded interval," *IEEE Trans. Antennas Propagat.*, vol. 43, pp. 614–622, June 1995.
[5] G. Oberschmidt, M. Behrens, and A. F. Jacob, "Comparison of spline-based wavelets for the analysis of microstrip lines," in *PIERS*, Innsbruck, Austria, July 1996, p. 581.
[6] K. F. Sabet, "Wavelet-based modeling of microwave circuits and antennas," presented at the Proc. Applicat. Wavelets Electromagnetics Workshop, San Francisco, CA, June 1996, ch. 3.
[7] S. G. Mallat, "A theory for multiresolution signal decomposition: The wavelet representation," *IEEE Trans. Pattern Anal. Machine Intell.*, vol. 11, pp. 674–693, July 1989.
[8] I. Daubechies, *Ten Lectures on Wavelets.* Philadelphia: SIAM, 1992.
[9] C. K. Chui and J. Z. Wang, "On compactly supported spline wavelets and a duality principle," *Trans. Amer. Math. Soc.*, vol. 330, no. 2, pp. 903–915, 1992.
[10] U. V. Gothelf and A. Østergaard, "Full-wave analysis of a two slot microstrip filter using a new algorithm for computation of the spectral integrals," *IEEE Trans. Microwave Theory Tech.*, vol. 41, pp. 101–108, Jan. 1993.
[11] R. H. Jansen and W. Wertgen, "A 3D field-theoretical simulation tool for the CAD of mm-wave MMIC's," *Alta Freq.*, vol. 47, no. 5, pp. 203–216, June 1988.
[12] T. K. Sarkar, Z. A. Marićević, and M. Kahrizi, "An accurate de-embedding procedure for characterizing discontinuities," *Int. J. Microwave Millimeter-Wave Computer-Aided Eng.*, vol. 2, no. 3, pp. 135–143, 1992.

# The Generalized TLM-Based FDTD Modeling of Frequency-Dependent and Anisotropic Media

Zhizhang Chen and Jian Xu

***Abstract*— A generalization of the previously proposed transmission-line matrix (TLM)-based finite-difference time-domain (FDTD) method is presented for modeling frequency-dependent and anisotropic media. The generalized scheme incorporates electric- and magnetic-flux densities in addition to variable mesh sizes. Since it is in an FD form, modeling techniques developed for the conventional FDTD can be easily adapted into the proposed TLM-based technique. In this paper, a modified $z$-transform technique for frequency-dependent media is implemented, and a two-dimensional (2-D) full-wave technique for guided-wave structures is developed. In all the FDTD computations, no conversions between the field quantities and TLM circuit parameters such as open- and short-circuited stubs are required.**

***Index Terms*—Anisotropic, FDTD, frequency dependent, TLM.**

## I. Introduction

Time-domain numerical methods have been shown to be powerful for solving electromagnetic related problems. These time-domain methods have received growing attention because of their versatility and simplicity. Two widely employed techniques so far are the finite-difference time-domain (FDTD) method of the Yee's grid [1] and the transmission-line matrix (TLM) method initially proposed by Johns [2]. The FDTD method is fairly easy to understand and implement, as it is the direct approximation of the Maxwell's equations. While the TLM, which uses the analogy between voltage and current waves in a transmission-line network and electromagnetic waves in space, is with less numerical dispersion. However, the TLM requires a conversion between the field quantities and circuit parameters to obtain the appropriate scattering matrix. For most of the cases, the conversions are not complicated, but sometimes they are not very straightforward and not easily understood, e.g., derivations of various impedances and open/short stub parameters related to variable grid sizes and medium inhomogeneity. To circumvent the problem, an FDTD and TLM combined technique—the TLM-based FDTD method equivalent to the TLM symmetrical condensed node—was proposed by Chen, Ney, and Hoefer [3], [4] while the work for the TLM expanded node was reported earlier by Voelker and Lomax [5].

The TLM-based FDTD is essentially the formulation of the TLM method in an FDTD fashion. It reveals the exact correspondence between the TLM and FDTD methods and the alternative ways of realizing the TLM concepts. Subsequent work on the more general correspondence was shown in [6]. The accuracy and dispersion comparisons between the TLM-based FDTD and the other FDTD schemes were presented in [7]. The TLM-based FDTD is found to have less numerical dispersion than the Yee's FDTD, but requires a little more memory space.

In this paper, the previously proposed TLM-based FDTD [3] is further exploited and generalized to include frequency dependence and anisotropics of a medium. Electromagnetic flux quantities are *directly* incorporated into the FDTD scheme and, therefore, a wide range of different media can be tackled. In this paper, frequency-dependent and anisotropic media are specifically treated. The successful applications of the technique shown in the following sections demonstrate the flexibility of the proposed FDTD method with its ease in adapting a different modeling scheme, e.g., the $z$-transform technique and the two-dimensional (2-D) full-wave technique. In all the proposed FDTD computations, no conversions between the field quantities and the TLM circuit parameters and stub-related operations are required. In addition, a normalizing procedure is also introduced to account for variable mesh sizes.

## II. The Generalization of the TLM-Based FDTD Formulation

In a general three-dimensional (3-D) case, Maxwell's curl equations in a stationary and sourceless medium can be expressed in the rectangular coordinates. For instance, for $D_x$ and $B_y$

$$\frac{\partial D_x}{\partial t} = \frac{\partial H_x}{\partial y} - \frac{\partial H_y}{\partial z} - \sigma_{ey} E_x \tag{1}$$

$$\frac{\partial B_y}{\partial t} = \frac{\partial E_z}{\partial x} - \frac{\partial E_x}{\partial z} - \sigma_{my} H_y \tag{2}$$

where $\sigma_e$ and $\sigma_m$ are, respectively, the equivalent electric and magnetic conductivities. Note that unlike the TLM-based FDTD developed so far, the flux densities are used in the equations.

Following the conventional notation, a function of the discretized space and time is denoted as

$$F(i\,\delta x,\, j\,\delta y,\, k\,\delta z,\, n\,\delta t) = F^n(i,\, j,\, k). \tag{3}$$

Manuscript received October 4, 1996; revised February 13, 1998. This work was supported in part by the Natural Sciences and Engineering Research Council of Canada.

Z. Chen is with the Department of Electrical and Computer Engineering, Daltech, Dalhousie University, Halifax, N.S., Canada B3J 2X4.
J. Xu is with Phase Atlantic Ltd., Moncton, N.B., Canada E1C 9N1.
Publisher Item Identifier S 0018-9480(98)03153-6.